THE ASTRONOMICAL JOURNAL, 120:2851–2858, 2000 December

A PROBABILISTIC QUANTIFICATION OF GALAXY CLUSTER MEMBERSHIP

R. J. BRUNNER AND L. M. LUBIN[1]
Department of Astronomy, California Institute of Technology, MC 105-24, 1201 East California Boulevard, Pasadena, CA 91125; rb@astro.caltech.edu
Received 2000 May 24; accepted 2000 August 17

ABSTRACT

Clusters of galaxies are important laboratories both for understanding galaxy evolution and for constraining cosmological quantities. Any analysis of clusters, however, is best done when one can reliably determine which galaxies are members of the cluster. While this would ideally be done spectroscopically, the difficulty in acquiring a complete sample of spectroscopic redshifts becomes rather daunting, especially at high redshift, when the background contamination becomes increasingly larger. Traditionally, an alternative approach of applying a statistical background correction has been utilized that, while useful in a global sense, does not provide information for specific galaxies. In this paper we develop a more robust technique that uses photometrically estimated redshifts to determine cluster membership. This technique can either be used as an improvement over the commonly used statistical correction method or it can be used to determine cluster candidates on an individual galaxy basis. By tuning the parameters of our algorithm, we can selectively maximize our completeness or, alternatively, minimize our contamination. Furthermore, our technique provides a statistical quantification of both our resulting completeness and contamination from foreground and background galaxies.

Key words: cosmology: observations — galaxies: distances and redshifts

1. INTRODUCTION

In the wake of the Hubble Deep Field campaigns (Williams et al. 1996) and with the growth of large photometric surveys (e.g., DPOSS and SDSS), the techniques involved in calculating photometric redshifts have become increasingly more sophisticated and precise (see Weymann et al. 1999 for a recent synopsis of the field). Accuracies of $\sigma_z = 0.05$ can be routinely achieved (Brunner, Connolly, & Szalay 1999). Therefore, it is now possible to use photometric redshifts to answer specific scientific questions (e.g., Connolly, Szalay, & Brunner 1998; Brunner, Connolly, & Szalay 2000). In light of this, we have begun a program to use accurate photometric redshifts to study the galaxy populations in high-redshift clusters of galaxies. For this study, we have examined the best-studied sample of optically selected, high-redshift clusters to date—that of Oke, Postman, & Lubin (1998). Over the past few years, Oke et al. (1998) have undertaken a detailed photometric, spectroscopic, and morphological survey of nine candidate clusters at $z \gtrsim 0.6$. The survey consists of deep $BVRIK'$ photometry, over 130 low-resolution Keck spectra per cluster field, and high spatial resolution Wide Field Planentary Camera 2 imagery from the *Hubble Space Telescope* (*HST*).

Previous work on similar galaxy cluster samples at various redshifts has relied on statistical corrections to remove contamination due to field galaxies when spectroscopic identifications are not available for all galaxies in the cluster field (e.g., Aragón-Salamanca et al. 1993; Lubin 1996; Smail et al. 1997; Dressler et al. 1997; Couch et al. 1998; Stanford, Eisenhardt, & Dickinson 1998; Lubin et al. 1998b). These types of corrections, however, are fraught with potential systematic effects, including cosmological variance, weak lensing, and sample selection criteria. While these effects serve only to increase the noise of any measurement made over a statistically complete sample, they systematically affect any measurement made on an individual cluster (e.g., the morphological fraction or the morphology-density relationship), introducing a bias into the actual measurement process. Furthermore, these line-of-sight contamination corrections apply to the entire galaxy sample and do not provide any information for specific galaxies. As a result, we have decided to explore the role that photometric redshifts could play in improving the reliability of identifying galaxy cluster members (Kodama, Bell, & Bower 1999; Lubin & Brunner 1999).

In this paper, we first describe in § 2 the details of the data observations, reduction, and catalog generation, emphasizing relevant points that are important for the estimation of photometric redshifts. In § 3, we describe the details of our redshift estimation technique. Next, we detail the cluster galaxy identification procedure in § 4. We conclude with a discussion of our results and future applications.

2. DATA

For the photometric redshift analysis, we have used the photometric and spectroscopic data from the original cluster survey of Oke et al. (1998). This survey consists of nine candidate clusters at redshifts $z \gtrsim 0.6$: Cl 0023+0423, Cl 0231+0048, Cl 0943+4804, Cl 1324+3011, Cl 1325+3009, Cl 1604+4304, Cl 1604+4321, Cl 1607+4109, and Cl 2157+0347. Oke et al. (1998) have determined that six of the nine candidate clusters are indeed real density enhancements, consistent with that of a cluster of galaxies. The observational data relevant for the work described in this paper consist of B-, V-, R-, I-, and K'-band imaging and spectroscopic observations of selected galaxies in each field.

2.1. *Observations and Data Reduction*

All the ground-based optical observations, both broadband and spectroscopic, were taken with the Low Resolution Imaging Spectrometer (LRIS; Oke et al. 1995) on either the Keck I or the Keck II 10 m telescopes. The infrared imaging was performed with the Infrared Imaging Camera (IRIM) on the Mayall 4 m telescope at Kitt Peak National Observatory. In this section, we briefly describe

[1] Hubble Fellow.

the observations and the data reduction; however, the reader is referred to Oke et al. (1998) for a complete account of these observations.

2.1.1. *Broadband Optical*

The photometric survey was conducted in four broadband filters, B, V, R, and I, which closely match the Cousins system. The response curves of these filters are shown in Figure 1 of Oke et al. (1998). In imaging mode, LRIS covers a field of view of $6' \times 8'$. The total exposure times in each filter are 3600, 2000, 1200, and 900 s for B, V, R, and I, respectively, and were chosen to give fairly uniform errors in the photometry. The B, V, and R observations consisted of two equal exposures to allow for accurate cosmic-ray rejection. The I exposure time was broken into three equal exposures to cope with the cosmic rays, as well as to avoid approaching the CCD saturation level.

The LRIS imaging data were reduced in the standard fashion. All frames were bias-subtracted, and pixel-to-pixel sensitivity variations were removed using dome flats. Large-scale gradients were removed by dividing each frame by a normalized two-dimensional spline fitted to the sky values in a sky flat. The sky flat was created by generating a median image from a stack of frames for each night and passband. For the I-band data, a two-dimensional fringe map was also created from the median filtered image by removing large-scale gradients within the median image. Fringing was removed from each I-band frame by subtracting a suitably scaled version of the fringe map.

Image registration for a given cluster field was performed by identifying approximately 10 unsaturated stars (detectable in all four passbands) to be used as astrometric reference points. The mean X and Y offsets of these stars in every frame taken of the cluster were computed relative to their locations in a fiducial B-band image. All image data for the cluster were shifted to match the B-band coordinate system, using a flux-conserving Lagrangian interpolation scheme to achieve registration at the subpixel level. Once all frames of a given cluster were registered to a common coordinate system, the independent exposures in each passband were co-added to produce the final four B, V, R and I images.

The Keck imaging has been calibrated to the standard Cousins-Bessell-Landolt (Cape) system through exposures of a number of Landolt standard-star fields (Landolt 1992). For a circular aperture with radius $3''$, the approximate limiting magnitudes are $B = 25.1$, $V = 24.1$, $R = 23.5$, and $I = 21.7$ for a $5\,\sigma$ detection.

2.1.2. *Spectroscopic*

Multislit observations of the cluster field were made with LRIS in spectroscopic mode using a 300 groove mm^{-1} grating blazed at 5000 Å. The chosen grating provided a dispersion of 2.35 Å pixel^{-1} and a spectral coverage of 5100 Å. The grating angle was set in to provide coverage from approximately 4400 to 9500 Å in the first order. A GG495 glass filter was used to eliminate the overlapping second-order spectrum; there is, therefore, no second-order contamination below 9700 Å. To obtain the full wavelength range along the dispersion axis, the field of view of the spectral observations was reduced from that of the imaging mode to approximately $2' \times 8'$.

Spectroscopic candidates were chosen from preliminary R-band imaging of each cluster field. All objects brighter than approximately $R = 23.5 \pm 0.1$ within the spectroscopic field of view of LRIS were included as candidates for slit mask spectra. For each cluster field, six different slit masks were made with approximately 30 objects per mask (including guide stars and duplicate observations). The exposure time for each mask was 1 hr. Flat-fielding and wavelength calibration were performed using internal flat-field and arc lamp exposures that were taken after each science exposure.

In practice, about 130 spectra per cluster field were acquired, with ~ 100 yielding measurable redshifts. A redshift measurement procedure that relies in part on visual inspection was used. The quality of the redshift identification was ranked by a number from 1 to 4, which roughly corresponds to the number of features used to identify the redshift. A quality of 4 means that the redshift is certain; a quality of 1 means that only one emission line was observed, and the redshift is only possible. Because the foreground and background contamination rate is so large at our cluster redshifts, approximately 50%–85% of the galaxies turn out to be field galaxies rather than cluster members (Oke et al. 1998; Postman, Lubin, & Oke 1998, 2000).

2.1.3. *Infrared*

Deep infrared imaging of the cluster sample was taken with IRIM, which contains a 256×256 NICMOS3 HgCdTe array and has a resolution of $0''.60$ pixel^{-1} on the 4 m telescope. The field of view ($154'' \times 154''$) covers the central region of each cluster. To make the deepest possible observations over this region, the entire LRIS field of view was not mosaicked. Observations were made in the 2.2 μm K' band. Each central field was observed using a 4×4 dither pattern with a step size of $10''$ and a total extent of $30''$. Each exposure had an effective exposure time of 1 minute, with four co-additions of individual, background-limited 15 s integrations. The total integration time on an individual cluster varied between 3 and 4.4 hr. Because the fields were not excessively crowded, we were able to use in-field dithering to create a global sky flat.

The K' cluster data were reduced using the Deep Infrared Mosaicing Software (DIMSUM), a publicly available package of IRAF scripts. This software generates not only a final stacked image, but also a corresponding exposure image, in which each pixel encodes the total number of seconds in the corresponding stacked image. This exposure image was appropriately scaled and used as a weight image by SExtractor during the catalog generation (see § 2.2).

The data were linearized, trimmed to exclude masked columns and rows on the edges of the arrays, and dark-subtracted using dark frames of the same exposure length as the observations. All images of a given night were flattened by a superflat made from a series of dome flats taken during the previous day. As part of the DIMSUM procedure, sky subtraction was done by subtracting a scaled median of nine temporally adjacent exposures for each frame. A first-pass reduction was used to create an object mask for each frame. This mask was created from a fully stacked mosaic image. It therefore excluded not only the bright objects but also those objects too faint to be detected in an individual exposure. In the second pass, the object mask was used to avoid object contamination of the sky flat in the production of sky frames. Final mosaicking of the images of each cluster were made with a replication of each pixel by a factor of 4 in both dimensions. This procedure conserves flux while eliminating the need for interpolation when the individual frames are co-aligned. A bad-pixel mask was used to exclude bad pixels from the final summed images.

Absolute photometric transformations were derived from the observations of Persson et al. (1998) *HST* standard stars. Each standard star was observed every night in five separate array positions. The observations of the standard stars were reduced in a manner similar to the cluster data (see Oke et al. 1998). An approximate limiting magnitude of $K' = 20$ for a 5 σ detection was reached in a standard aperture of radius 3.″0.

2.2. *Catalog Generation*

We used SExtractor version 2.1.5 (Bertin & Arnouts 1996) to perform the source detection and photometry because this program is able to detect objects in one image and analyze the corresponding pixels in a separate image. Applied uniformly to multiband image data (i.e. using the same detection image for all measurement images), this method produces a matched aperture photometric catalog. We generated an optimal detection image from the *B*, *V*, *R*, and *I* images using a χ^2 process (Szalay, Connolly, & Szokoly 1999). Briefly, this process involves convolving each input image with a Gaussian kernel matched to the seeing. The convolved images were squared and normalized so that they have zero mean and unit variance. The four processed images (corresponding to the original *B*, *V*, *R*, and *I* images) were co-added, forming the χ^2 detection image.

To determine the optimal threshold parameters for source detection, we compared a histogram of the pixel distribution in the χ^2 image with a χ^2 function with four degrees of freedom. (This distribution theoretically corresponds to the background pixel distribution for our co-added χ^2 image.) By taking the difference (pixel − theory) between the two histograms, we generated the histogram of pixel values that were due to the objects we were trying to detect. We defined the Bayesian detection threshold as the intersection of the sky (or theoretical prediction) and object pixel distributions (i.e., where the object pixel flux becomes dominant). To convert this empirical threshold for use with SExtractor, we scaled the χ^2 threshold (in flux per pixel) into a surface brightness threshold (in magnitudes per square arcsecond).

The infrared images were cataloged separately because of their radically different field of view and pixel scale. The catalog was generated using SExtractor as before but in single-image mode (i.e., the detection image was also the measurement image). To maximize the number of detections, we utilized the exposure image generated by DIMSUM during the data reduction (see § 2.1.3) to provide a weight map to determine object parameters properly in an image with varying signal-to-noise ratio (due to the different total integration times in different pixels).

All our resultant analyses use the total magnitudes calculated by SExtractor. The optical magnitudes were, by design, matched apertures, which reduces the scatter in any photometric redshift technique. Since the K'-band images were not co-registered with the optical images, the aperture can be slightly different. However, since the total apertures were rather large in angular extent, any aperture effects on our resulting analysis should be small ($\lesssim 0.02$ mag) compared with the more dominant effects of photometric errors.

2.3. *Cross-Identifications*

The last step in preparing these data for analysis was to combine the optical imaging, near-infrared imaging, and the spectroscopic observations into a single data set for each cluster field. Since the original spectroscopic targets were determined from a separate catalog, we first cross-matched the spectroscopic catalog with the optical catalog using a growing annulus technique in which the angular distance ψ was determined using the formula

$$\psi = \arccos\left[\sin\phi_s \sin\phi_p + \cos\phi_s \cos\phi_p \cos(\theta_s - \theta_p)\right],$$

where the angles (θ and ϕ indicate declination and right ascension, respectively) have been properly converted into radians, the subscript *s* refers to spectroscopic targets, and the subscript *p* refers to photometric objects. In all cases, the match occurred for very small angles because spectroscopic targets were selected from the optical images.

The cross-identification between the infrared and optical catalogs, however, was slightly more complicated, although it was done in an identical manner. This was due to the different telescopes and detectors used during the observations and the corresponding geometric distortions between the two catalogs. Furthermore, the variation of the spectral energy distributions between the *I* and K' bands for the sources in our sample can be quite large, especially for galaxies at relatively high redshift. As a result, some objects in each catalog remained unmatched below the angular limit, which is approximately the confusion beam width (approximately 5″).

3. EMPIRICAL PHOTOMETRIC REDSHIFT

The technique that we have developed for determining cluster membership requires redshift estimates for all galaxies in the field. Although this technique is independent of the actual redshift estimation technique, we have used the empirical photometric redshift technique (Brunner et al. 1999) to generate redshift estimates for all galaxies in our sample. This is the result of the simplicity of the empirical technique in determining redshifts for a photometric sample of galaxies for which an adequate training set exists. Furthermore, the empirical technique, since it is based only on the data under investigation, is more robust than alternative techniques to uncertainties in the spectral energy distributions of galaxies. These alternative techniques, such as template-based methods, could also be used, as long as a realistic estimate of the error in the estimated redshift can be determined.

The empirical photometric redshift technique requires a calibration sample to determine the coefficients of the empirical relation. For this work, we have used the spectroscopic data that was acquired as part of the original observational campaign to determine the cluster velocity dispersions (Postman et al. 1998, 2000). The reliability (i.e., the inverse of the intrinsic error) of a spectroscopic redshift is generally quite high, with quoted errors often measured in tenths of 1% (i.e., $\delta < 0.001$). In reality, however, a redshift is accurate only when the spectral identification is also accurate. As a result, we restricted the spectroscopic calibrators to include only objects with redshifts that are determined by at least two spectral lines, i.e., a quality of 2 or higher (for details, see Postman et al. 1998). The next step was to restrict the sample to those objects that were below the 10% photometric error limit, that did not have bad detection flags (e.g., object near edge of frame or incomplete aperture data), and that were below our high-redshift cutoff of $z = 1.5$. We also removed one additional galaxy that, having an E and A spectrum (Dressler & Gunn 1983, 1992;

Zabludoff et al. 1996), skewed the results of our calibration for normal galaxy spectra (the dominant population in our sample). The final spectroscopic calibration data consisted of 130 galaxies from five different cluster fields.

With the final calibration sample, we determined a fourth-order polynomial fitted to the four magnitudes, B, R, I, and K', and the spectroscopic redshift. The number in our sample of 130 calibrators is nearly twice the number of coefficients required (a fourth-order polynomial in four variables has 70 coefficients); we are, therefore, properly constraining the degrees of freedom when determining the coefficients of our polynomial fit. From Figure 1, there are no obvious systematic variations in our calculated relationship, which has an intrinsic dispersion (the standard deviation of the residual differences for the calibrating sample) of $\sigma_z = 0.072$. In addition, the distribution of the residuals (see Fig. 2) is approximately Gaussian in shape.

3.1. *Estimating Photometric Redshift Errors*

To reliably determine cluster membership, we also need to have an estimate for the error in our photometric redshift calculation. While the measurement of the intrinsic dispersion in our relationship provides one estimate (which is commonly used throughout the relevant literature; see, e.g., Kodama et al. 1999), we have also developed an alternative, extrinsic estimate. Briefly, the intrinsic error is calculated directly from any available spectroscopic redshifts; that is, it is simply the dispersion in the derived relationship between spectroscopic and photometric redshifts. Extrinsic errors, on the other hand, are calculated in a Monte Carlo fashion, accounting for all known measurement uncertainties.

Following Brunner et al. (1999), we derive extrinsic redshift error estimates for all galaxies in our data set using a Monte Carlo technique to simulate our uncertainty in the observables (i.e., flux measurements), as well as our sampling of the galaxy distribution in the B, R, I, and K' four-dimensional flux space. Specifically, we use a bootstrap with replacement algorithm to draw a new set of random calibrating galaxies from the original training set. This algorithm allows for duplicate galaxy entries and is designed to emphasize any incompleteness in the sampling of the true distribution of galaxies in the four-dimensional space B, R, I, and K' by the calibration redshifts. Furthermore, the magnitudes of the newly derived calibrating sample were drawn from a Gaussian probability distribution function with the mean given by the measured magnitude and σ by the magnitude error. This accounts for any uncertainties in the flux measurements.

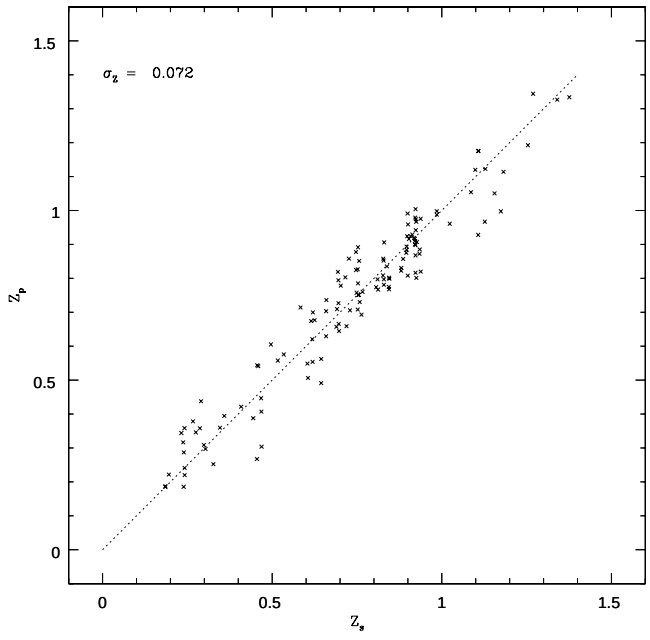

FIG. 1.—Correlation between the photometric and spectroscopic redshifts for the entire calibration sample. The straight line is of unit slope and is not a fit to the actual data.

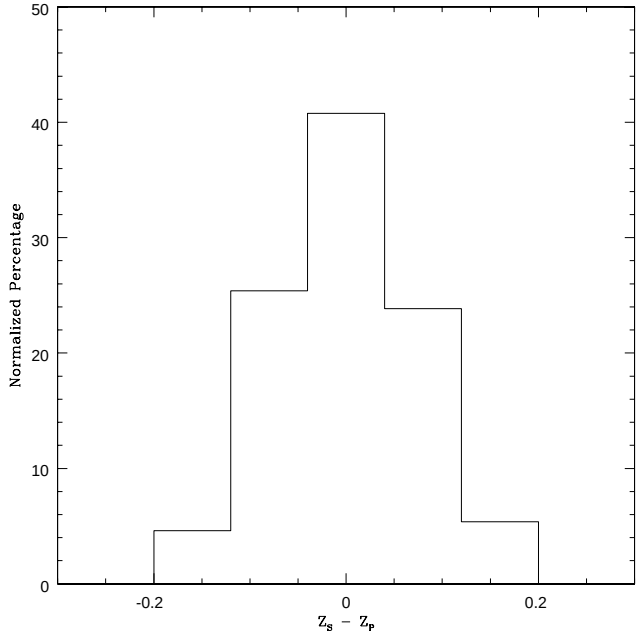

FIG. 2.—Histogram of the residual differences between photometric and spectroscopic redshifts for the entire calibration sample, which is approximately Gaussian in shape. The bin width was chosen to approximate the measured intrinsic dispersion in our relationship.

This technique was used to generate 100 different realizations of the photometric redshift relationship. For each different realization (all of which form our ensemble), a photometric redshift was calculated for every galaxy in the photometric catalog. As a result, this produced 100 different redshift estimates for each galaxy. By applying a quantile cut, we can approximate the redshift distribution for each individual galaxy by a Gaussian. Therefore, the error in the photometric redshift for each object was defined by $\sigma_z = (Q_5 - Q_2)/2.0$, where Q_5 and Q_2 refer to the fifth and second quantiles of the distribution of each galaxy's estimated redshift, respectively (see Brunner et al. 1999). Together, our original photometric redshifts and redshift error estimates completely define the photometric redshift distribution separately for each galaxy.

Of the two types of redshift error estimates, the intrinsic error is by far the most commonly used (e.g., Kodama et al. 1999) as it is the easiest to calculate. The extrinsic error, however, does a better job of quantifying the actual error in the redshift estimate of an individual galaxy, which can be either smaller or considerably larger than the intrinsically estimated global error (see Fig. 15 in Brunner et al. 1999). Fundamentally, the extrinsic method provides a separate error estimate for each galaxy, while the intrinsic method provides only a global estimate.

4. CLUSTER MEMBERSHIP

While the optimal technique for unambiguously determining cluster membership is to obtain spectroscopic redshifts for all sources in the field, this process can be prohibitively expensive in telescope time allocation, especially at relatively high redshifts ($z > 0.5$). As a result, many previous studies (e.g., Aragón-Salamanca et al. 1993; Lubin 1996; Smail et al. 1997; Dressler et al. 1997; Couch et al. 1998; Stanford et al. 1998; Lubin et al. 1998b) have utilized a background contamination estimator to statistically quantify both the number of galaxies that belong to a given cluster and the morphological fraction of the cluster members. In addition to possible systematic effects that are implicit in using techniques of this type, background corrections provide no information on the likelihood of an individual galaxy being a member of a cluster.

Photometric redshifts, however, provide a relatively inexpensive redshift estimate; therefore, they can be used to estimate cluster redshifts (see, e.g., Gal et al. 2000) and to determine likely cluster members (Kodama et al. 1999; Lubin & Brunner 1999). Previous techniques to select cluster members based on photometric redshifts (e.g., Kodama et al. 1999) are based on a simplistic technique for defining galaxy cluster members. Basically, any galaxy that lies within a redshift shell centered on the redshift of the galaxy cluster (i.e., $z_c \pm \delta_z$) is identified as a member. Because photometric redshifts have a large uncertainty (generally a factor of 10 to 50 higher than spectroscopic redshifts), a large redshift shell (e.g., $\delta_z \approx 0.05$) is used to identify likely cluster members. While certainly useful, this approach does not provide a reliable means for identifying line-of-sight contaminating galaxies.

As a result, we have developed an alternative technique that relies on the probabilistic interpretation of a photometric redshift to determine cluster membership. We define the probability density function, $\Phi(z)$, for an individual galaxy's redshift as a Gaussian probability distribution function with mean, μ, given by the estimated photometric redshift and standard deviation, σ, defined by the estimated error in the photometric redshift.

$$\Phi(z) = (1/\sigma\sqrt{2\pi})e^{-(z-\mu)^2/2\sigma^2}$$

Using this interpretation, we can calculate the probability that a galaxy has an actual redshift within a given redshift interval.

$$\begin{aligned} P(\text{cluster} \mid z_c, \Delta z, \mu, \sigma) &= N \int_{z_c-(1/2)\ \Delta z}^{z_c+(1/2)\ \Delta z} \Phi(z)dz\ , \\ &= N \int_{z_c-(1/2)\ \Delta z}^{z_c+(1/2)\ \Delta z} \frac{1}{\sigma\sqrt{2\pi}}\, e^{-(z-\mu)^2/2\sigma^2} dz\ , \\ &= \frac{N}{2}\left[\gamma\left(\frac{1}{2}, z_H\right) - \gamma\left(\frac{1}{2}, z_L\right)\right], \end{aligned}$$

where N is a suitable normalization factor, z_c is the cluster redshift, Δz is the width in redshift space that you are sampling, the limits of integration are

$$z_H = \frac{(z_c + \frac{1}{2}\Delta z) - \mu}{\sqrt{2}\sigma}, \quad z_L = \frac{(z_c - \frac{1}{2}\Delta z) - \mu}{\sqrt{2}\sigma}\ ,$$

and γ is the incomplete gamma function. [Of course, $\gamma(1/2, z)$ is also known as the error function, erf(z)].

Within this formalism, the only undeclared quantity is σ or, alternatively, the uncertainty in the estimated redshift for a given galaxy. In our framework, this value can be determined either from the intrinsic error in our photometric redshift relation or in a separately calculated extrinsic error. As a result, this approach is strongly dependent on the actual technique used to estimate the photometric redshift error and the corresponding redshift error. In this paper, we have applied this technique using empirically derived photometric redshifts since we have a well-defined calibration data set of spectroscopic redshifts. Empirically defined photometric redshifts are much less sensitive to uncertainties in the shape and the evolution with redshift of the spectral energy distribution of galaxies than competing techniques such as template photometric redshifts (Brunner 1997).

On the other hand, the method we have introduced can easily be adapted to work with alternative redshift estimation procedures, including template photometric redshift algorithms, by utilizing the derived dispersion estimate. The empirically based techniques do have shortcomings, most notably, the requirement of a high-quality training set and the fundamental limitation that any resultant analysis is limited to the same region of flux space delineated by the training set of calibration redshifts. In our case, the spectroscopic survey of Oke et al. (1998) provides a wonderful training set, which completely samples the region in flux space that encompasses the vast majority of cluster galaxies. When this is not the case, template-based photometric redshift estimation methods, which can be applied to data for which there are no calibrators, are required. In this case, however, extreme care must be used to minimize any systematic effects, such as morphological variation of the redshift error estimates or template incompleteness.

By using the calibration galaxies as a training set, we can empirically determine the optimal probability value that provides the threshold for cluster membership. This can be tuned to either maximize the completeness or minimize contamination. In this paper, our sample is small enough that a simple visual threshold determination is sufficient; however, there is no reason a more powerful maximum likelihood or regression analysis technique could not be employed, especially for larger data sets (e.g., the SDSS). Furthermore, additional information (such as evolutionary color tracks) can be used to select likely cluster members that can be used to provide a bootstrap estimator for the probability threshold.

As a demonstration of this technique, we have applied this procedure to the data described earlier in this paper. We consider two clusters from our survey (see § 2 for more information); the first is Cl 0023+0423, at redshift $z = 0.84$ (Postman et al. 1998; Lubin, Postman, & Oke 1998a; Lubin et al. 1998b), and the second is Cl 1604+4321, at redshift $z = 0.92$ (Postman et al. 2000; Lubin et al. 2000). These two clusters provide a useful demonstration because the first cluster is well sampled by our data set, while the second cluster pushes the photometric limits of our data. Since the utility of this technique is so strongly dependent on the exact method used for estimating the redshift and redshift error for every galaxy in the field, we have intentionally relegated a more nearly complete discussion of the application of this technique to our own data to a later, more focused paper (Lubin et al. 2000).

In Figures 3 and 4, we display the results of applying this

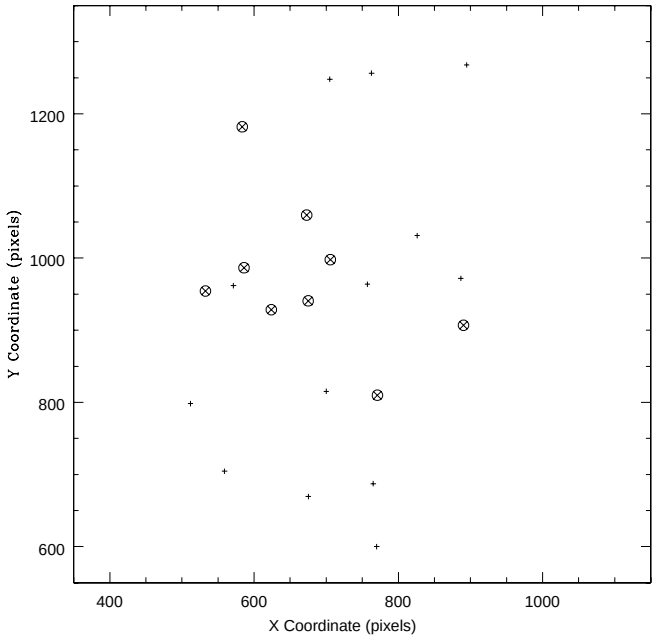

FIG. 3.—. Plot of results for the field of Cl 0023+0423, displaying the locations of calibrating galaxies in the image (the pixel scale is 0″.215 pixel^{-1}) and indicating spectroscopically confirmed cluster members (*circles*), photometrically classified cluster members (*crosses*), and field galaxies (*plus signs*) that are additional calibrators for the photometric redshift relation. With the probability cut selected for this figure, we have 100% completeness and 0% contamination.

technique to the spectroscopic targets in the Cl 0023+0423 cluster field, as well as the full photometric sample for this field. In both cases, we used the intrinsic error of the photometric redshift relationship as our redshift error. From Figure 3, we clearly do quite well (i.e., 100% completeness with no contamination). Of course, translating this success to the full sample is not guaranteed; however, as long as our calibration sample adequately samples the four-dimensional flux space occupied by the galaxies in our full sample (i.e., we have a fair and unbiased training set), there is no reason to expect significant variation from these results.

In Figures 5 and 6, we show the results of applying this technique to the spectroscopic targets in the Cl 1604+4321 cluster field, as well as to the entire photometric sample for this cluster. This time, however, we have used the extrinsic error, which is calculated independently for each galaxy. By judiciously selecting the probability threshold, we can maximize the completeness ($\approx$88%), while minimizing the contamination ($\approx$21%). While we would clearly prefer full completeness and no contamination, this cluster demonstrates one of the strengths of our technique, namely, its ability to quantify both our completeness and our contamination empirically.

In fact, our technique predicts 37 cluster members within the field of view of our combined image (see Fig. 6). If we use the predictions of deep number counts (e.g., Driver et al. 1995); Smail et al. 1995; Abraham et al. 1996) to estimate the contamination due to foreground and background galaxies, we estimate there should be 33 ± 14 cluster members in the image (note the large uncertainty in this statistical calculation), which is the exact number that we find after correcting for contamination and incompleteness [i.e., $37(100\% - 21\%)/88\% = 33$]. We have made this comparison with the statistical background correction simply to show that we are finding a reasonable number of cluster galaxies; however, unlike the background correction tech-

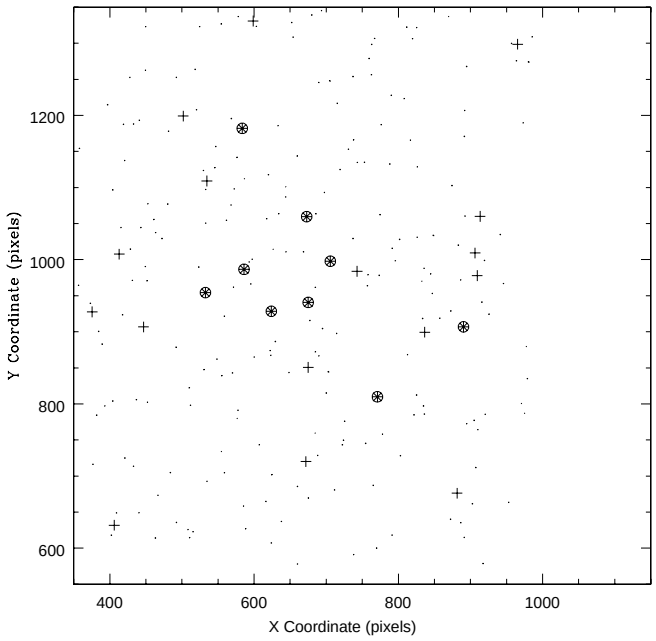

FIG. 4.—Results for the field of Cl 0023+0423, demonstrating the application of this technique to the full photometric catalog. Cluster candidates are indicated as in Fig. 1 (both spectroscopic and photometric), while new cluster candidates are indicated by plus signs and general field galaxies are indicated by dots. After correcting for contamination and incompleteness, the number of cluster members determined through our photometric redshift technique agrees with the number predicted by statistically correcting for background counts.

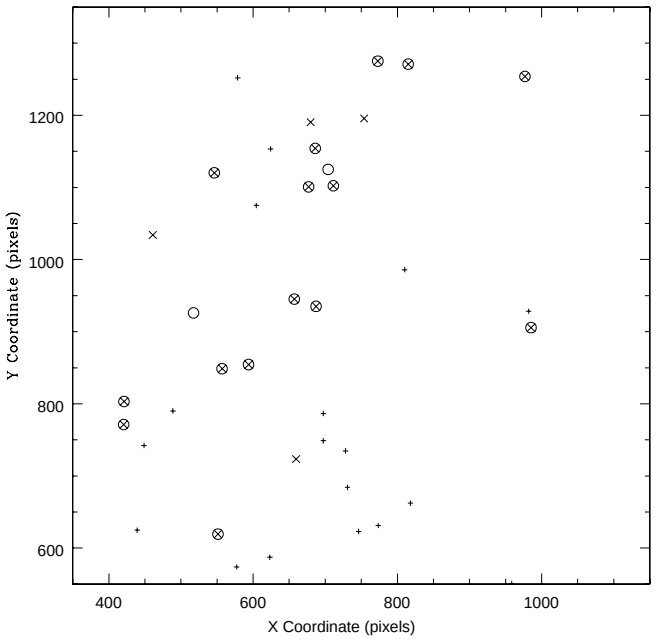

FIG. 5.—Plot of results for the field of Cl 1604+4321, displaying the locations of calibrating galaxies in the image (the pixel scale is 0″.215 pixel^{-1}) and showing spectroscopically confirmed cluster members (*circles*), photometrically classified cluster members (*crosses*), and field galaxies (*plus signs*) that are additional calibrators for the photometric redshift relation. With the probability cut selected for this figure, we have $\approx$88% completeness and $\approx$21% contamination.

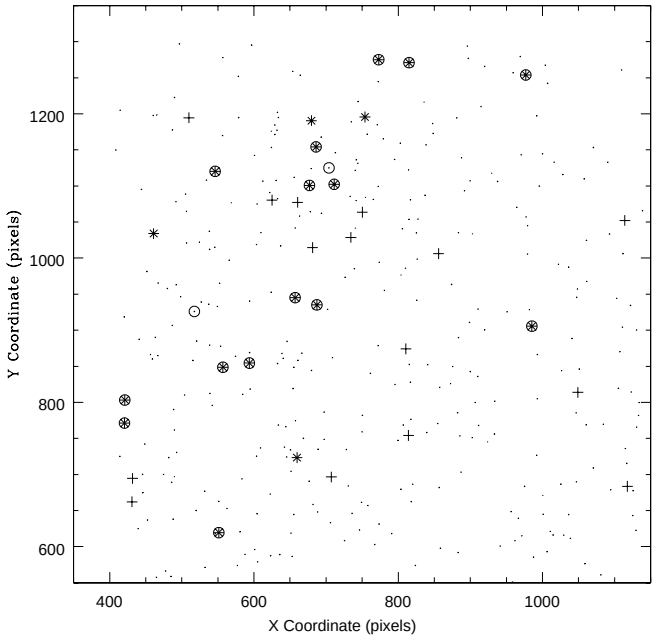

FIG. 6.—Results for the field of Cl 1604+4321, demonstrating the application of this technique to the full photometric catalog. Cluster candidates are indicated as in Fig. 1 (both spectroscopic and photometric), while new cluster candidates are indicated by plus signs and general field galaxies are indicated by dots. After correcting for contamination and incompleteness, the number of cluster members determined through our photometric redshift technique agrees with the number predicted by statistically correcting for background counts.

nique, we have explicitly identified the likely cluster members.

5. DISCUSSION

In this paper, we have presented a novel technique for the probabilistic determination of cluster membership based solely on photometric redshift and redshift error estimates. Our technique can be tuned either to maximize the completeness of cluster member identification (i.e., identify all actual cluster members) or, alternatively, to minimize the contamination due to foreground and background galaxies in the field. Furthermore, this technique provides a robust estimation for both the completeness and contamination fractions of identified cluster members as a function of likelihood. A comparison between our new technique with the traditional technique of statistical background correction shows remarkable agreement, with the advantage that our technique actually identifies the galaxies which are cluster members.

The results in this paper are based on an empirical photometric redshift estimation, which we have used because (1) we have a reliable training set from our extensive spectroscopic survey and (2) these photometric redshifts are less sensitive to uncertainties in spectral evolution that can affect other redshift estimation techniques. Alternative redshift estimation techniques, however, can easily be incorporated into the algorithm, as all that is needed is a redshift estimate and a corresponding redshift error estimate. In the case of template photometric redshifts, the redshift error could be determined from either the intrinsic dispersion in the photometric redshift relation, an interpolation over the χ^2 goodness-of-fit parameter, or even more appropriately through a combination of the χ^2 parameter and a Monte Carlo bootstrap approach to mimic photometric uncertainty and template incompleteness. In this case, however, caution must be used to minimize any possible systematic effects that might depend on various fundamental assumptions, such as the spectral type.

The only free parameter in the entire technique is the probability threshold used to determine cluster membership. Optimally, as we have done in this paper, a training set of spectroscopically confirmed cluster members can be used to set the threshold value empirically. When this is not the case, alternative techniques, such as color selection to identify the early-type sequence at the appropriate redshift, can be used to identify likely cluster candidates. On the other hand, the expected number of cluster candidates can be calculated from the statistical background correction arguments. This expected number of cluster members can be used as an independent estimator as we can set the probability threshold value to reproduce the estimated number of cluster galaxies.

Based on our work, we believe that photometric redshifts are an ideal way to study the galaxy populations in high-redshift clusters. For a large number of the tests of common cluster properties (e.g., the morphology-density relationship), this method eliminates the need for extensive spectroscopic surveys and the uncertainty of estimating the background contamination. As an additional example of the utility of this approach, consider the magnitude-limited spectroscopic survey used in this analysis. We can approximate the total number of spectroscopic targets observed by multiplying the number of clusters used in this analysis (five) by the approximate number of targets per cluster field (130), implying that a total of 650 objects were observed spectroscopically. The redshift identification success rate was nearly 77%. Of these redshifts, 50%–85% belong to noncluster galaxies. These numbers imply that the spectroscopic survey was only 12%–38% efficient in identifying cluster candidates, depending on the richness of the cluster.

In addition, our technique provides the ability to tune the cluster candidate identification either to maximize the completeness or, alternatively, to minimize the contamination. As a practical example, maximizing completeness is essential for any observational program that is designed to completely sampling the cluster (e.g., spectroscopic targeting). On the other hand, minimizing contamination is important for selecting a characteristic set of cluster members for a detailed study of cluster member properties (e.g., the morphological fraction or the morphology-density relationship; Lubin et al. 2000). Furthermore, if a training set of spectroscopically confirmed galaxies is available, we can actually characterize the percentages of both the completeness and contamination that we expect in our final cluster candidate catalog.

Like any photometric redshift based technique, our technique is limited in its efficacy by the quality of the photometric data used in the analysis. However, our technique can be applied by using a variety of photometric redshift estimation methods. Therefore, we expect that, in the near future, we will be able to utilize fully the capabilities of this technique for cluster research.

We are very grateful to Bev Oke and Marc Postman for the enormous time and effort that they put into obtaining and reducing all of the data used in this paper. We also wish

to thank the anonymous referee for a thorough reading of the original paper and many interesting comments. This research has made use of the NASA Astrophysics Data System Abstract Service. L. M. L. is supported by NASA through Hubble Fellowship grant HF-01095.01-97A from the Space Telescope Science Institute, which is operated by the Association of Universities for Research in Astronomy, Inc., under NASA contract NAS 5-26555.

REFERENCES

Abraham, R. G., van den Bergh, S., Glazebrook, K., Ellis, R. S., Santiago, B. X., Surma, P., & Griffiths, R. E. 1996, ApJS, 107, 1
Aragón-Salamanca, A., Ellis, R. E., Couch, W. J., & Carter, D. 1993, MNRAS, 262, 764
Bertin, E., & Arnouts, S. 1996, A&AS, 117, 393
Brunner, R. J. 1997, Ph.D. thesis, Johns Hopkins Univ.
Brunner, R. J., Connolly, A. J., & Szalay, A. S. 1999, ApJ, 516, 563
———. 2000, ApJ, in press
Connolly, A. J., Szalay, A. S., & Brunner, R. J. 1998, ApJ, 499, 125L
Couch, W. J., Barger, A. J., Smail, I., Ellis, R. E., & Sharples, R. M. 1998, ApJ, 497, 188
Dressler, A., & Gunn, J. E. 1983, ApJ, 270, 7
———. 1992, ApJS, 78, 1
Dressler, A., et al. 1997, ApJ, 490, 577
Driver, S. P., Windhorst, R. A., Ostrander, E. J., Keel, W. C., Griffiths, R. E., & Ratnatunga, K. U. 1995, ApJ, 449, 23L
Gal, R. R., de Carvalho, R. R., Brunner, R., Odewahn, S. C., & Djorgovski, S. G. 2000, AJ, 120, 540
Kodama, T., Bell, E. F., & Bower, R. G. 1999, MNRAS, 302, 152
Landolt, A. U. 1992, AJ, 104, 340
Lubin, L. M. 1996, AJ, 112, 23
Lubin, L. M., & Brunner, R. J. 1999, in ASP Conf. Ser. 191, Photometric Redshifts and High Redshift Galaxies, ed. R. Weymann, L. Storrie-Lombardi, M. Sawicki, & R. Brunner (San Francisco: ASP), 173
Lubin, L. M., Postman, M., & Oke, J. B. 1998a, AJ, 116, 643
Lubin, L. M., Postman, M., Oke, J. B., Brunner, R. J., Gunn, J. E., Hoessel, J. G., & Schneider, D. P. 2000, AJ, in preparation
Lubin, L. M., Postman, M., Oke, J. B., Ratnatunga, K. U., Gunn, J. E., Hoessel, J. G., & Schneider, D. P. 1998b, AJ, 116, 584
Oke, J. B., et al. 1995, PASP, 107, 375
Oke, J. B., Postman, M., & Lubin, L. M. 1998, AJ, 116, 549
Persson, S. E., Murphy, D. C., Krzeminski, W., Roth, M., & Rieke, M. J. 1998, AJ, 116, 2475
Postman, M., Lubin, L. M., & Oke, J. B. 1998, AJ, 116, 560
———. 2000, in preparation
Smail, I., Dressler, A., Couch, W. J., Ellis, R. E., Oemler, A., Butcher, H., & Sharples, R. M. 1997, ApJS, 110, 213
Smail, I., Hogg, D. W., Yan, L., & Cohen, J. C. 1995, ApJ, 449, 105L
Stanford, S. A., Eisenhardt, P. R., & Dickinson, M. 1998, ApJ, 492, 461
Szalay, A. S., Connolly, A. J., & Szokoly, G. P. 1999, AJ, 117, 68
Weymann, R., Storrie-Lombardi, L., Sawicki, M., & Brunner, R. 1999, ed. ASP Conf. Ser. 191, Photometric Redshifts and High Redshift Galaxies (San Francisco: ASP)
Williams, R. E., et al. 1996, AJ, 112, 1335
Zabludoff, A. I., Zaritsky, D., Lin, H., Tucker, D., Hashimoto, Y., Shectman, S. A., Oemler, A., & Kirshner, R. P. 1996, ApJ, 466, 104